A Journal of the Gesellschaft Deutscher Chemiker

Angewandte International Edition Chemie

GDCh

www.angewandte.org

Accepted Article

Title: From Symmetry Breaking to Unraveling Chirality of Metal Nanoclusters

Authors: Guocheng Deng, Sami Malola, Juanzhu Yan, Ying-Zi Han, Peng Yuan, Chaowei Zhao, Xiting Yuan, Shuichao Lin, Zichao Tang, Boon K. Teo, Hannu Häkkinen, and Nanfeng Zheng

To be cited as: *Angew. Chem. Int. Ed.* 10.1002/anie.201800327
Angew. Chem. 10.1002/ange.201800327

Link to VoR: http://dx.doi.org/10.1002/anie.201800327
http://dx.doi.org/10.1002/ange.201800327

WILEY-VCH

10.1002/anie.201800327

WILEY-VCH

COMMUNICATION

From Symmetry Breaking to Unraveling Chirality of Metal Nanoclusters

Guocheng Deng,[a] Sami Malola,[b] Juanzhu Yan,[a] Yingzi Han,[a] Peng Yuan,[a] Chaowei Zhao,[a] Xiting Yuan,[a] Shuichao Lin,[a] Zichao Tang,[a] Boon K. Teo*,[a] Hannu Häkkinen,[b] Nanfeng Zheng*[a]

Abstract: A general method, using mixed ligands (here diphosphines and thiolates) is devised to turn an achiral metal cluster, $Au_{13}Cu_2$, into an enantiomeric pair by breaking (lowering) the overall molecular symmetry with the ligands. Using an achiral diphosphine, a racemic $[Au_{13}Cu_2(DPPP)_3(SPy)_6]^+$ was prepared which crystallizes in centrosymmetric space groups. Using chiral diphosphines, enantioselective synthesis of an optically pure, enantiomeric pair of $[Au_{13}Cu_2((2r,4r)/(2s,4s)\text{-}BDPP)_3(SPy)_6]^+$ was achieved in one pot. Their circular dichroism (CD) spectra give perfect mirror images from 250-500nm with maximum anisotropy factors of 1.2×10^{-3}. Density Functional Theory (DFT) calculations provided good correlations with the observed CD spectra of the enantiomers and, more importantly, revealed the origin of the chirality. Racemization studies show high stability (no racemization at 70°C) of these chiral nanoclusters, which hold great promise in applications such as asymmetry catalysis.

Chirality is ubiquitous in nature[1, 2] and plays a key role in enantioselective catalysis, pharmaceutical sciences, optical devices, etc.[3-6] In the past few decades, people have established lots of chemical means for enantioselective synthesis of chiral molecules for specific applications.[7-10] To date, many chiral nanoclusters have been discovered or synthesized. Atomically precise nanoclusters are particularly good models to probe the origin of chirality. Many efforts have been dedicated to unraveling the chirality in cluster science and several plausible mechanisms have been proposed such as the dissymmetric field effect and chiral footprint model.[11-15] However, unlike chiral organic compounds or other small molecules, asymmetric synthesis of large chiral structures such as nanoparticles or nanoclusters remains a real challenge, which hampers the progress of unraveling chirality of metal nanoclusters.

Generally speaking, chiral nanoclusters can be classified into three broad categories by different origins of the chirality: (1) chiral metal core; (2) asymmetry arrangement of achiral surface structure (such as RS-Au-SR unit); (3) homochiral ligands induced extrinsic chirality.[16-21] Some chiral clusters may belong to two of the three categories, e.g., with chirality originating from both staple and kernel.[22, 23] Symmetry breaking is a universal phenomenon in nature and the concept of *symmetry breaking* in the present context includes spontaneous resolution, chirality amplification, chiral induction, asymmetric catalysis, crystal growth, or combinations thereof.[24, 25] Since most metal clusters have an achiral, highly symmetrical metal core (often possessing mirror or inversion symmetries), the simplest method to synthesize a chiral metal cluster is to lower the overall symmetry with the ligands. However, symmetry breaking by asymmetry arrangement of achiral ligands is often difficult to control. Furthermore, it inevitably leads to racemic mixtures. Many efforts have been made to enantioseparate those racemic mixtures by using chiral HPLC columns and phase transfer method using a chiral ammonium salt.[26-29] The problem here is that it is often challenging to carry out such separations to produce optically pure nanoparticles. Moreover, racemization can exist in chiral metal cluster systems. For example, racemization studies on thiolate-protected gold cluster have been done by Bürgi's group. They found the gold−thiolate interface is flexible and racemization phenomenon have been observed at 30°C.[30, 31]

Herein we report the syntheses of three closely related, extrinsically chiral metal nanoclusters via these two strategies. The first is a racemate, characterized as $[Au_{13}Cu_2(DPPP)_3(SPy)_6]^+$ (**2**), which has an achiral metal core, six Spy, and three achiral diphosphine ligands DPPP in asymmetric arrangements (where Spy= pyridine-2-thiol and DPPP=1,3-bis(diphenyphosphino)propane). Using chiral (2r,4r)/(2s,4s)-2,4-bis(diphenylphosphino)pentane (BDPP) (Figure S1) in place of achiral diphosphine, two optically pure enantiomers $[Au_{13}Cu_2(2r,4r\text{-}BDPP)_3(SPy)_6]^+$ (**3-R**) and $[Au_{13}Cu_2(2s,4s\text{-}BDPP)_3(SPy)_6]^+$ (**3-S**), were obtained in one pot. All the three clusters were synthesized by reducing a mixture of Au, Cu, pyridinethiol and diphosphine with $NaBH_4$ in an ice bath (see Supporting Information (SI) for more details). Single crystals suitable for X-ray diffraction were grown by slow solvent evaporation after ten days.

Single-crystal structure determination revealed that **2** is a racemate crystallized in the centrosymmetric space group $P2_1/c$. The unit cell comprises two pairs (Z = 4) of enantiomers (Table S1 and Figure S2). As shown in Figure 1a, the molecular architecture of **2** is similar to the previously reported $[Au_{13}Cu_2(PPh_3)_6(SPy)_6]^+$ (**1**, depicted in Figure S3).[32] As shown in Figure 1b and c, **2** has an icosahedral Au_{13} core and two Cu atoms capping two Au_3 triangles of the icosahedral Au_{13} core oriented along one of the 3-fold axes of the icosahedral Au_{13}. The core of **2** is achiral and displays D_{3d} symmetry. The six pyridine-2-thiol ligands bind to the two Cu atoms and six gold (one each) atoms from the two Au_3 triangles capped by Cu as bidentate ligands (Figure 1a). The pyridine-2-thiol ligands in two sides of the metal core rotate some degree (Figure 1d and Table 4). The pyridine-2-thiol ligands are in asymmetry arrangement and displays C_3 symmetry. So the symmetry of this cluster is effectively lowered here. Three DPPP ligands bind to six Au atoms at the 'equatorial' positions of the icosahedral core. As shown in Figures 1e, the three DPPP ligands cap on the cluster

[a] G. C. Deng, J. Z. Yan, Y. Z. Han, P. Yuan, Dr. C. W. Zhao, X. T. Yuan, Dr. S.C. Lin, Prof. Z. C. Tang, Prof. B. K. Teo, Prof. N. F. Zheng
State Key Laboratory for Physical Chemistry of Solid Surfaces, Collaborative Innovation Center of Chemistry for Energy Materials, and Department of Chemistry, College of Chemistry and Chemical Engineering, Xiamen University
Xiamen 361005, China
E-mail: nfzheng@xmu.edu.cn
boonkteo@xmu.edu.cn
[b] Dr. S. Malola, Prof. H. Häkkinen
Departments of Physics and Chemistry
Nanoscience Center, University of Jyväskylä
Jyväskylä 40014, Finland

Supporting information for this article is available on the WWW under http://

10.1002/anie.201800327

in two different types(gray and pale blue). So the three DPPP ligands display C_1 symmetry. The point-group symmetry of **2** has been "broken" (lowered) by pyridine-2-thiol and DPPP ligands "step by step" from D_{3d} to C_3 then to C_1.

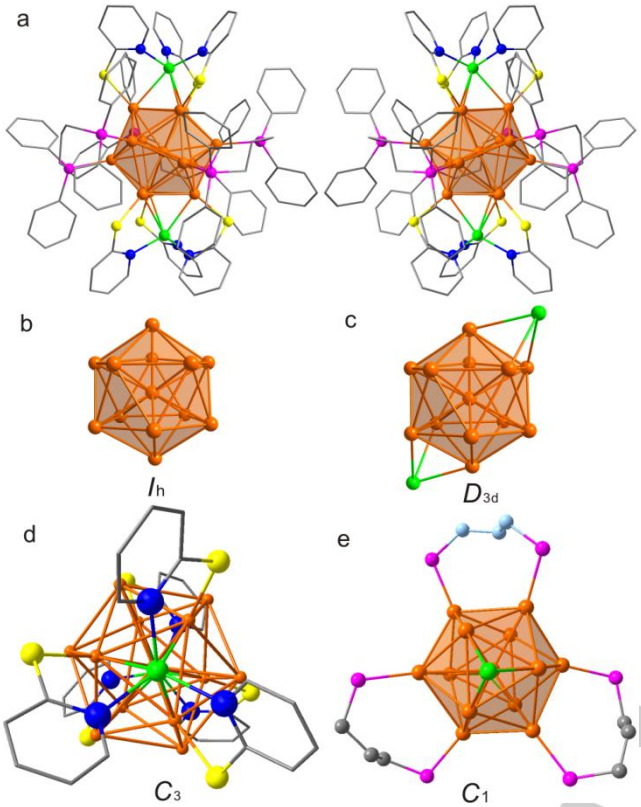

Figure 1. a) Molecular structure of the $[Au_{13}Cu_2(DPPP)_3(SPy)_6]^+$ enantiomer pair (left: **2-R**; right: **2-S**). Symmetry breaking from I_h of Au_{13} b) to D_{3d} of $Au_{13}Cu_2$ c) to C_3 of $Au_{13}Cu_2(SPy)_6$ d) to C_1 of $[Au_{13}Cu_2(DPPP)_3(SPy)_6]^+$ e). Color codes: orange, Au; green, Cu; pink, P; yellow, S; blue, N; gray and pale blue, C. All hydrogen atoms are omitted for clarity.

Detailed analysis of the molecular architecture of **2** revealed that the $Au_6(DPPP)_3$ units on the 'equatorial' positions of the cluster have different types in different enantiomers (Figure S4). The DPPP ligands cap on the enantiomer pair in two different conformations, which due to the "flexibility" of the C-C-C in DPPP ligands. The types of the $Au_6(DPPP)_3$ unit "locking" the rotate direction of the six pyridine-2-thiol ligands. Since the DPPP is achiral, two conformations corresponding to an enantiomeric pair coexist in the crystal structure, giving rise to the racemate **2**.

Based on this analysis, it occurs to us that we should be able to use a chiral diphosphine to restrain the "flexibility" of the C-C-C between the two phosphorus atoms to "lock" the arrangement of pyridine-2-thiol ligands, and then realize enantioselective synthesis of chiral metal cluster in one pot. The strategy adopted here is to use chiral diphosphine ligands (2s,4s)-BDPP and (2r,4r)-BDPP in place of achiral DPPP. The steric hindrance of two chiral C atoms on the propyl group of (2s,4s)-BDPP or (2r,4r)-BDPP should restrict the relative rotations of the alkyl group. Single crystal analysis revealed that the resulting metal cluster were **3-R** and **3-S** (Table S2 and S3). As shown in Figure 2, two enantiomers exhibit perfect mirror symmetry. To the best of our knowledge, this is the first report of enantioselective synthesis of a chiral cluster exhibiting 100% optical purity, and as we shall show later, the chirality can be attributed to the lowering of the centrosymmetric symmetry of the achiral metal core by the peripheral ligands. The methodology adopted here may have applicaions in other fields as well. In this regard, an earlier example in which a pair of racemic mixtures, D,L-camphorates, were spontaneously resolved into chirally opposite MOFs bears some resemblance to the present methodology.[33]

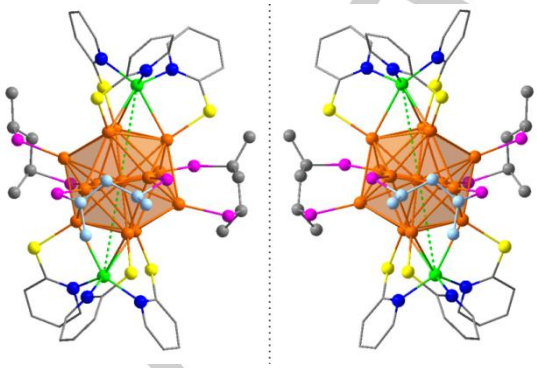

Figure 2. Overview of **3-R** (left) and **3-S** (right). Color codes: orange, Au; green, Cu; pink, P; yellow, S; blue, N; gray and pale blue, C. All hydrogen atoms and benzene rings are omitted for clarity.

The degree of twisting of the pyridyl groups can be measured as twist angles θ_n of the top and θ_n' (n=1-3) of the bottom N atoms with reference to the Au_{13} core (viewed along the Cu-Au-Cu principal C_3 symmetry axis) (Figure S5). The results are listed in Table S4 with the average twist angle designated as θ_N. Likewise the twist angles for S and P atoms can be obtained and the average values are listed as θ_S and θ_P, respectively, in Table S4. The asymmetry in the arrangements of the N, S, and P atoms can now be gauged by the deviation of the parameter $\Delta\theta = \theta - \theta'$ values from either 0º or 60º, as listed in Table S4. For $\Delta\theta$ = 0º, the six respective atoms (N, S, or P atoms) conform to idealized D_{3h} point-group symmetry whereas for $\Delta\theta$ = 60º, they instead conform to idealized D_{3d} point-group symmetry. Both have mirror planes and are therefore achiral. It follows that chirality may occur for asymmetric arrangements of the N, S, or P ligands in the region of $0º<\Delta\theta<60º$. Indeed, an examination of Table S4 revealed, within each cluster, the measured $\Delta\theta$ values follow the trend of $\Delta\theta_N>\Delta\theta_S>\Delta\theta_P$ signifying that the asymmetry in the arrangements of these atoms decreases in this order. So from structure analysis, we can conclude that pyridine-2-thiol ligands at the poles of the cluster are mainly responsible for most of the chirality, which consistent with the DFT calculation. Structural analysis revealed that there are many van der Waals interactions between the pyridinethiol and phosphine ligands (see Table S5), as well as between phosphine ligands (Table S6). These interactions suggest that the asymmetric arrangement of the peripheral ligands, as well as the conformational difference of the diphosphine ligands, may be due to the steric hindrance among the ligands (Figure S6).

As shown in the UV-vis spectra of their pure crystals and crude products in CH_2Cl_2 (Figure 3a and S7), **2** and **3-R** exhibit three strong bands at 331, 408 and 464 nm, and a weak shoulder peak at 550 nm. Calculated UV-vis spectra are consistent with the experiment except a small systematic red shift of about 0.3-0.4 eV. Both products were also characterized by electrospray ionization mass spectrometry (ESI−MS) in CH_2Cl_2. As depicted in Figures 3b and S8, all clusters are +1 charged (positive mode used in the ESI−MS analysis) 8-electron superatoms, which also can be confirmed by DFT calculations.

10.1002/anie.201800327

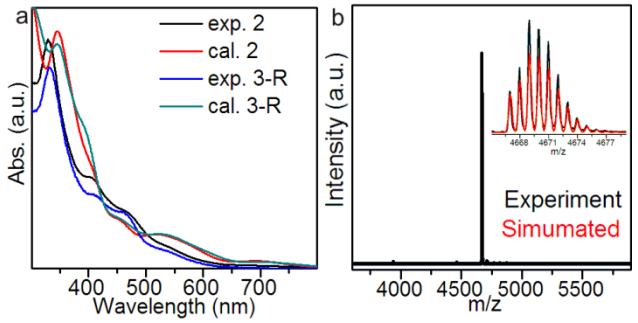

Figure 3. a) Experimental and computed UV−vis spectra of **2** and **3-R** in CH_2Cl_2. In the theoretical spectra, the individual optical transitions have been folded into a smooth curve by using a Gaussian width of 0.1 eV. b) ESI−MS of single-crystals of **3-R** in CH_2Cl_2.

As shown in Figure 4a, the circular dichroism (CD) spectra of optically pure CH_2Cl_2 solutions of **3-R** and **3-S** give perfect mirror images from 250 to 500nm and eight clear signals (minima or maxima: 279, 288, 297, 319, 334, 360, 395, and 465nm) are observed. Anisotropy factors g = ΔA/A = θ [mdeg] / (32980 × A) were calculated over the spectral range and a maximum anisotropy factor of up to 1.2×10^{-3} at 360 nm was obtained (Figure 4b). For racemization studies, the crystal of **3-R** was dissolved in DMF. The intensity of the CD signal at 358 nm was followed over the course of 30 min at four different temperatures (40, 50, 60 and 70°C). Result shown that the cluster quite stable and no racemization phenomenon have been observed at 70°C (Figure 4c). The UV−vis spectra of **3-R** before and after racemization studies are very similar which shows that decomposition is negligible (Figure S9), and is quite different with Bürgi's work.[30, 31] The UV−vis spectra of **3-R** in CH_2Cl_2 have no obvious change in air after one month at room temperature (Figure S10). The intensities of the CD signals decrease with increasing temperature, due mainly to a change in the absorbance of the solution as a whole.

As shown in Figure 4d, the calculated CD spectrum of **3-R** is 0.3-0.4 eV red shifted as compared to the experimental one, though the features are comparable. From both spectra, eight distinguishable features, including maxima and minima, can be identified and are labeled accordingly. It is interesting to explore theoretically the contributions of the electronic states to the CD peaks in term of localization. Rotatory strength transition contribution map (RTCM) analysis of the labeled features in the CD-spectrum are shown in Figures S11 and S12 for **3-R**. Analysis of occupied states and unoccupied states with regards to the electronic excitations of **3-R** are shown in Figure S13. The calculation results show that electronic states localized on pyridine-2-thiol ligands are the most important contributors to the chirality as a result of the structural distortion of these ligands, breaking the reflection and inversion symmetries of the metal $Au_{13}Cu_2$ core, as described above. The pyridinethiol ligands, collectively, act as chiral centers of the cluster whereas the effects of the overall arrangement of the pyridine ligands and the binding configurations are inherited through the delocalization of the electronic states as well as to organic part of the pyridine ligands and to the nearby Au- and Cu-atoms. The role of the electronic states on phosphine ligand are minimal at best, and only in the low energy features of the CD-spectrum. A comparison of the CD-spectra of the three $Au_{13}Cu_2$ clusters, **1-R** to **3-R,** with different phosphine ligands provides a better understanding of the origin of the chirality. The major differences in the CD-spectra of the clusters having either BDPP, DPPP or PPh_3 ligands are observed at the low energies above 500 nm (Figure S14), which is however not resolved experimentally). At higher energies (below 500 nm), the features of the CD spectra of the three clusters with different phosphine ligands resemble one another. This is consistent with the above interpretation that the pyridinethiol ligands on the cluster are mainly responsible for the chirality. Effects of the phosphine ligands on chirality, if any, can therefore only be indirect by creating spatial restrictions for the pyridines due to interactions and overall arrangement of the ligands on the surface.

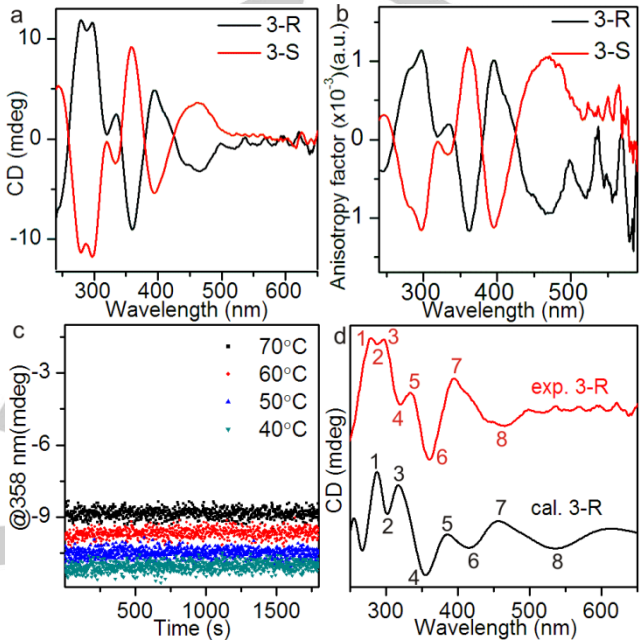

Figure 4. a) Circular dichroism (CD) spectra of enantiomers of **3-R** and **3-S**. b) Corresponding anisotropy factors of **3-R** and **3-S** enantiomers (g = A/A of up to 1.2×10^{-3}). c) The response of racemization experiment of **3-R** at 358 nm as a function of time at different temperatures in DMF solution. d) Comparison of the experimental (in red) and calculated (in black) CD-spectra of **3-R**.

In conclusion, we have synthesized and structurally characterized three closely related chiral metal nanoparticles. A general methodology, using mixed surface ligands (diphosphines and thiolates in this paper) to break (lower) the symmetry of the achiral metal core in order to transform it into a chiral cluster is devised and experimentally demonstrated. The interaction between the phosphine and thiolate ligands results in the asymmetric arrangement of the surface ligands, thereby giving rise to the chirality. Using chiral diphosphines in place of achiral diphosphines, it was demonstrated that enantioselective synthesis of chiral nanoclusters, namely, the enantiomeric pair $[Au_{13}Cu_2((2r,4r)/(2s,4s)\text{-BDPP})_3(SPy)_6]^+$, can be accomplished with 100% optical purity and high yield in a one-pot synthesis. The asymmetric arrangement of the pyridinethiol (Spy) ligands was caused by steric hindrance in their weak interactions with the phosphine ligands, as manifested in the *breaking* of the reflection and inversion symmetries of the achiral metal core. The effect follows the trend of (chiral BDPP) > (achiral DPPP) > PPh_3. DFT calculations allowed detailed assignments of the CD peaks. Finally, the high stability of these chiral nanoclusters hold great promise in applications such as asymmetry catalysis, biomedicine, etc.

Experimental Section

Synthesis of 2: For a typical synthesis of **2**, 12 mg $AuSMe_2Cl$ and 8.4 mg DPPP were dissolved in the mixture solution of methanol and dichloromethane. After the solution was cooled to 3 °C, 24 mg $Cu(OAc)_2$ and 14 mg pyridine-2-thiol were added. After 20 minutes stirring, 1 ml $NaBH_4$ aqueous solution (20 mg/ml) and 50 μl triethylamine were added quickly to above mixture under vigorous stirring. The reaction was aged for 12 hours at 3 °C. The aqueous phase was then removed. The mixture in organic phase was centrifuged for 3 min at 10000 r/min. And then the yellow precipitate was discarded and the organic phase was washed several times with water. Black block crystals were obtained through slow solvent evaporation after 10 days.
Synthesis of 3: Same as **2** with the exception of use 8.8 mg (2r,4r)/(2s,4s)-BDPP in place of 8.4 mg DPPP. Black block crystals were obtained through slow solvent evaporation after 10 days.

Acknowledgements

We thank the MOST of China (2017YFA0207302, 2015CB932303) and NNSF of China (21731005, 21420102001, 21390390, 21333008) for financial support. B.K.T. acknowledges financial support from iChEM, Xiamen University. The computational work in the University of Jyväskylä was supported by the Academy of Finland (project 266492 and H.H.'s Academy Professorship). S.M. and H.H. thank Lauri Lehtovaara for implementation of the RTCM analysis into the GPAW software.

Keywords: chirality• nanocluster• enantiosynthesis• CD spectrum

[1] W. J. Lough, I. W. Wainer, *Chirality in natural and applied science*, CRC Press/Wiley-Blackwell Pub., Osney Mead, Oxford, OX ; Boca Raton, **2002**.
[2] L. D. Barron, *Space Sci. Rev.* **2008**, *135*, 187-201.
[3] H. Zhang, D. E. Zelmon, L. Deng, H.-K. Liu, B. K. Teo, *J. Am. Chem. Soc.* **2001**, *123*, 11300-11301.
[4] T. Mallat, E. Orglmeister, A. Baiker, *Chem. Rev.* **2007**, *107*, 4863-4890.
[5] K. Taniguchi, R. Maeda, T. Ando, T. Okumura, N. Nakazawa, R. Hatori, M. Nakamura, S. Hozumi, H. Fujiwara, K. Matsuno, *Science* **2011**, *333*, 339-341.
[6] R. Philip, P. Chantharasupawong, H. Qian, R. Jin, J. Thomas, *Nano Lett* **2012**, *12*, 4661-4667.
[7] K. Soai, T. Shibata, H. Morioka, K. Choji, *Nature* **1995**, *378*, 767-768.
[8] R. Oda, I. Huc, M. Schmutz, S. J. Candau, F. C. MacKintosh, *Nature* **1999**, *399*, 566-569.
[9] H. Häkkinen, M. Moseler, O. Kostko, N. Morgner, M. A. Hoffmann, B. Issendorff, *Phys. Rev. Lett.* **2004**, *93*, 093401.
[10] W. Ma, L. G. Xu, A. F. de Moura, X. L. Wu, H. Kuang, C. L. Xu, N. A. Kotov, *Chem. Rev.* **2017**, *117*, 8041–8093.
[11] C. Gautier, T. Burgi, *J. Am. Chem. Soc.* **2006**, *128*, 11079-11087.
[12] C. Gautier, T. Bürgi, *J. Am. Chem. Soc.* **2008**, *130*, 7077-7084.
[13] H. Yao, *Curr. Nanosci.* **2008**, *4*, 92-97.
[14] H. Yao, T. Fukui, K. Kimura, *J. Phys. Chem. C* **2008**, *112*, 16281-16285.
[15] M. Z. Zhu, H. F. Qian, X. M. Meng, S. S. Jin, Z. K. Wu, R. C. Jina, *Nano Lett.* **2011**, *11*, 3963-3969.
[16] P. D. Jadzinsky, G. Calero, C. J. Ackerson, D. A. Bushnell, R. D. Kornberg, *Science* **2007**, *318*, 430-433.
[17] S. Knoppe, T. Bürgi, *Acc. Chem. Res.* **2014**, *47*, 1318-1326.
[18] S. Takano, T. Tsukuda, *J. Phys. Chem. Lett.* **2016**, *7*, 4509-4513.
[19] J. Z. Yan, H. F. Su, H. Y. Yang, C. Y. Hu, S. Malola, S. C. Lin, B. K. Teo, H. Häkkinen, N. F. Zheng, *J. Am. Chem. Soc.* **2016**, *138*, 12751-12754.
[20] I. Chakraborty, T. Pradeep, *Chem. Rev.* **2017**, *117*, 8208-8271.
[21] H. Yang, J. Yan, Y. Wang, G. Deng, H. Su, X. Zhao, C. Xu, B. K. Teo, N. Zheng, *J. Am. Chem. Soc.* **2017**, *139*, 16113-16116.
[22] L. Liao, S. Zhuang, C. Yao, N. Yan, J. Chen, C. Wang, N. Xia, X. Liu, M.-B. Li, L. Li, X. Bao, Z. Wu, *J. Am. Chem. Soc.* **2016**, *138*, 10425-10428.
[23] C. J. Zeng, Y. X. Chen, C. Liu, K. Nobusada, N. L. Rosi, R. C. Jin, *Sci. Adv.* **2015**, *1*, e1500045.
[24] R. E. Morris, X. Bu, *Nat. Chem.* **2010**, *2*, 353-361.
[25] L. Feng, Z. Wong, R. Ma, Y. Wang, X. Zhang, *Science* **2014**, *346*, 972-975.
[26] I. Dolamic, S. Knoppe, A. Dass, T. Burgi, *Nat. Commun.* **2012**, *3*, 798.
[27] S. Knoppe, I. Dolamic, A. Dass, T. Buergi, *Angew. Chem. Int. Ed.* **2012**, *51*, 7589-7591.
[28] C. Zeng, T. Li, A. Das, N. L. Rosi, R. Jin, *J. Am. Chem. Soc.* **2013**, *135*, 10011-10013.
[29] S. Knoppe, O. A. Wong, S. Malola, H. Häkkinen, T. Bürgi, T. Verbiest, C. J. Ackerson, *J. Am. Chem. Soc.* **2014**, *136*, 4129-4132.
[30] S. Knoppe, I. Dolamic, T. Bürgi, *J. Am. Chem. Soc.* **2012**, *134*, 13114-13120.
[31] N. Barrabés, B. Zhang, T. Burgi, *J. Am. Chem. Soc.* **2014**, *136*, 14361-14364.
[32] H. Y. Yang, Y. Wang, J. Lei, L. Shi, X. H. Wu, V. Makinen, S. C. Lin, Z. C. Tang, J. He, H. Hakkinen, L. S. Zheng, N. F. Zheng, *J. Am. Chem. Soc.* **2013**, *135*, 9568-9571.
[33] S. Chen, J. Zhang, X. Bu, *Inorg. Chem.* **2009**, *48*, 6356-6358.
[34] CCDC 1814031-1814033 contain the supplementary crystallographic data for this paper. These data are provided free of charge by The Cambridge Crystallographic Data Centre.

10.1002/anie.201800327

WILEY-VCH

Entry for the Table of Contents

COMMUNICATION

Using mixed ligands, diphosphines and pyridinethiol, an achiral metal cluster, $Au_{13}Cu_2$, can be turned into an enantiomeric pair by breaking the reflection and inversion symmetries (thereby lowering the molecular symmetry): chiral diphosphines allow one-pot enantioselective synthesis of enantiomers with 100% optical purity. Temperature-dependent racemization studies showed high chirality stability (up to 70°C). DFT calculations revealed the origin of the chirality.

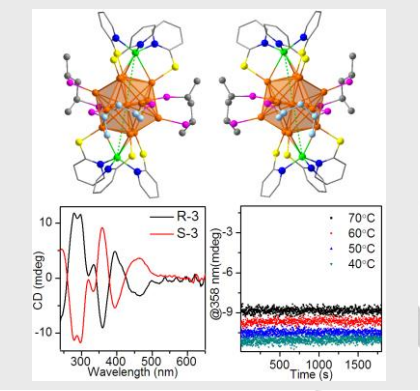

Guocheng Deng, Sami Malola, Juanzhu Yan, Yingzi Han, Peng Yuan, Chaowei Zhao, Xiting Yuan, Shuichao Lin, Zichao Tang, Boon K. Teo, Hannu Häkkinen, Nanfeng Zheng**

Page No. – Page No.

From Symmetry Breaking to Unraveling Chirality of Metal Nanoclusters